CATALYSIS

The state of zinc in methanol synthesis over a Zn/ZnO/Cu(211) model catalyst

Peter Amann[1]†, Bernhard Klötzer[2], David Degerman[1], Norbert Köpfle[2]‡, Thomas Götsch[3], Patrick Lömker[4,1], Christoph Rameshan[5], Kevin Ploner[2], Djuro Bikaljevic[2], Hsin-Yi Wang[1], Markus Soldemo[1]§, Mikhail Shipilin[1], Christopher M. Goodwin[1], Jörgen Gladh[1]§, Joakim Halldin Stenlid[1]¶, Mia Börner[1], Christoph Schlueter[4], Anders Nilsson[1]*

The active chemical state of zinc (Zn) in a zinc-copper (Zn-Cu) catalyst during carbon dioxide/carbon monoxide (CO_2/CO) hydrogenation has been debated to be Zn oxide (ZnO) nanoparticles, metallic Zn, or a Zn-Cu surface alloy. We used x-ray photoelectron spectroscopy at 180 to 500 millibar to probe the nature of Zn and reaction intermediates during CO_2/CO hydrogenation over Zn/ZnO/Cu(211), where the temperature is sufficiently high for the reaction to rapidly turn over, thus creating an almost adsorbate-free surface. Tuning of the grazing incidence angle makes it possible to achieve either surface or bulk sensitivity. Hydrogenation of CO_2 gives preference to ZnO in the form of clusters or nanoparticles, whereas in pure CO a surface Zn-Cu alloy becomes more prominent. The results reveal a specific role of CO in the formation of the Zn-Cu surface alloy as an active phase that facilitates efficient CO_2 methanol synthesis..

Methanol receives much interest as an industrial chemical as well as for its potential as an energy carrier (*1*). Its gravimetric energy density is comparable to that of liquid ammonia and can easily be distributed and stored with established technologies. To date, the leading industrial catalyst for the CO/CO_2 hydrogenation toward methanol consists of a mixture of Cu, ZnO, and Al_2O_3 (*2*). Methanol synthesis is carried out between 150° and 300°C at pressures of 50 to 100 bar but can also occur at substantially lower pressures of a few millibar (*3*).

Although this catalytic process is a century old, years of intense research have aimed to determine the mechanism and active sites. The catalytic nature of the Zn in the catalyst is still highly debated (*2*), and the mechanism is not yet fully experimentally verified. The addition of ZnO/Zn goes beyond the role of a mere particle dispenser and acts as a chemically active promoter of the reaction (the ZnCu synergistic effect). There are a number of hypotheses about the chemical state of Zn—more specifically, whether it is in a metallic state as a surface alloy (*4*) or a bulk alloy (*5*), and whether small ZnO islands are present on the surface (*6*, *7*) or in bulk forms (*8*, *9*). There is also a proposal that mixed phases could coexist, either in the bulk or on the surface (*10*). Additionally, Zn diffusion and Zn spillover on the Cu surface have been observed at various conditions, suggesting that the system can have a strongly dynamic character (*4*, *11*). These highly divergent hypotheses result from a complex interplay between Cu and ZnO and the relative proportions of CO_2 and CO in the reactant gas and thus have sparked intense debate (*12*, *13*).

Another mechanistic issue is whether the Zn-promoted mechanism propagates through

[1]Department of Physics, Stockholm University, AlbaNova University Center, 10691 Stockholm, Sweden. [2]Institute of Physical Chemistry, University of Innsbruck, Innrain 52c, 6020 Innsbruck, Austria. [3]Department of Inorganic Chemistry, Fritz Haber Institute of the Max-Planck Society, Faradayweg 4-6, 14195 Berlin, Germany. [4]Photon Science, Deutsches Elektronen-Synchrotron DESY, Notkestr. 85, 22607 Hamburg, Germany. [5]Institute of Materials Chemistry, Technische Universität Wien, Getreidemarkt 9/BC/01, 1060 Vienna, Austria.
***Corresponding author. Email: andersn@fysik.su.se**
†Present address: Scienta Omicron AB, Danmarksgatan 22, 75323 Uppsala, Sweden.
‡Present address: Plansee SE, Metallwerk-Planseestraße 71, 6600 Reutte, Austria.
§Present address: PULSE Institute, SLAC National Accelerator Laboratory, 2575 Sand Hill Road, Menlo Park, CA 94025, USA.
¶Present address: SUNCAT Center for Interface Science and Catalysis, SLAC National Accelerator Laboratory, 2575 Sand Hill Road, Menlo Park, CA 94025, USA.

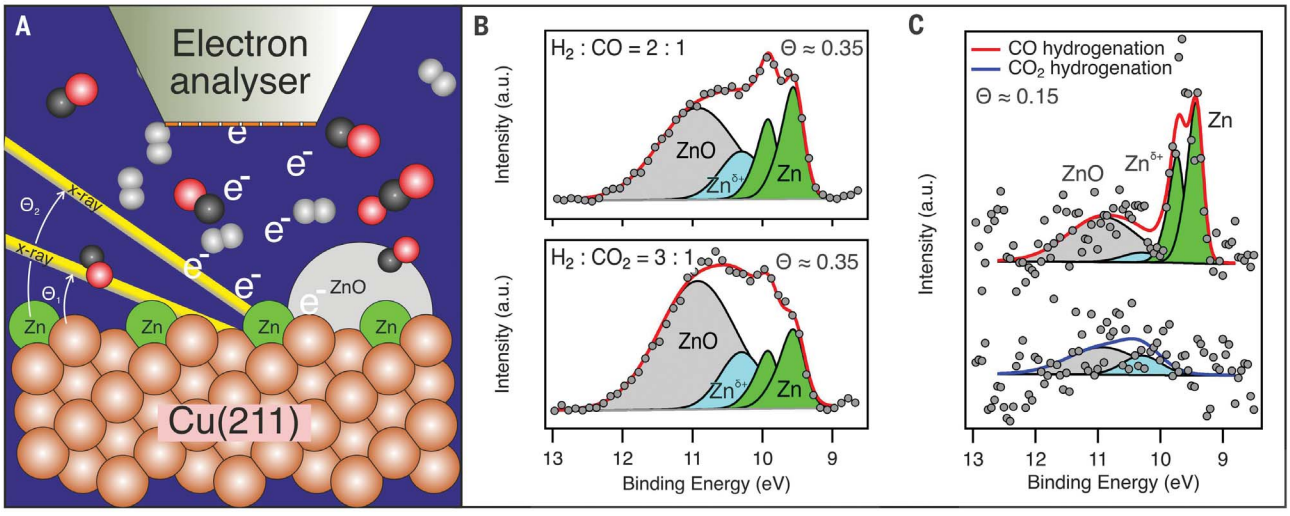

Fig. 1. Experimental setup and x-ray photoelectron spectra under different gas environments. (**A**) The surface of Zn/ZnO/Cu(211) is probed with grazing incidence x-rays at different angles (Θ_1 and Θ_2) while the surface is exposed to an elevated pressure of a gas mixture of CO, CO_2, and H_2. The surface was heated from the backside to achieve reaction conditions. (**B**) Experimental x-ray photoelectron spectra of the Zn 3d region obtained at 180 mbar, 140°C, and stoichiometric gas composition, using 4750 eV of photon energy. The experiment was conducted at ~35% surface Zn. The relative amount of ZnO to metallic Zn shows a strong dependency on gas composition. a.u., arbitrary units. (**C**) Experimental x-ray photoelectron spectra of the Zn 3d region obtained at 500 mbar, 230°C, and H_2:CO = 2.6:1 and H_2:CO_2 = 2.6:1, using 4600 eV of photon energy at a Zn coverage of ~15%. The spectra contain more noise because of the elevated pressure but exhibit more-pronounced differences between the two gas compositions.

formate and methoxy species as stable intermediates with different propensities, depending on whether the reactants are CO_2, CO, or a mixture of both (*4*, *6*, *14*, *15*). It has been determined from isotope labeling experiments that the reaction proceeds more efficiently from CO_2 than CO (*16*), but it remains unresolved how the mixture of the two gases yields the highest production rate of methanol (*17*). However, the cooperative action of ZnO_x and CO_2 has also been reported to enhance the rate of methanol synthesis from CO, even when the CO_2 fraction is as low as 3% (*18*).

Experimental observation of the response from the potential active sites and surface intermediates in situ could test the various hypotheses about the active catalytic site, but such studies would need to be conducted near the operating conditions at which the reaction turns over (*19*). As the catalyst is exposed to elevated temperatures and pressures with a variable reaction mixture, it may undergo critical changes that take place only in the uppermost atomic layers. In many cases, only a few active centers at step edges are responsible for reaction propagation (*20*). Active centers and reaction intermediates often amount to minority species in a dominating macroscopic bulk system of the catalyst material together with a large macroscopic gas volume. To meet this challenge, recent studies have conducted in situ x-ray absorption spectroscopy of the Cu-Zn system at high-pressure conditions (*8*–*10*), but only with the use of bulk-sensitive detection schemes.

X-ray photoelectron spectroscopy (XPS) can be used to investigate the chemical nature of catalytic surfaces and adsorbates through core-level shifts. In particular, all aspects of the catalyst system in terms of the metallic/oxide surface, adsorbates, and gas phase can be probed under identical conditions (*21*), and well-defined peaks are often observed. The high inelastic scattering cross section of photoelectrons in the gas phase makes vacuum conditions necessary. The approach for catalysis studies using XPS has either been postreaction analysis after the reaction at high pressure or under near–ambient-pressure conditions with a differential pumping arrangement (*22*).

Near–ambient-pressure conditions in the 1-mbar regime are still limited in terms of high-pressure capability when reactions proceed at high rates (*23*). For the Cu-Zn system, the pressure has been restricted to between 0.05 and 1 mbar (*7*, *10*, *24*). Nakamura *et al.* have pointed out that postreaction studies can potentially result in misleading conclusions about the active state of Zn in methanol synthesis (*12*), in which reaction intermediates [e.g., formate (HCOO)] may decompose and oxidize the surface when the system is evacuated and the temperature is reduced. Kuld *et al.* (*3*) and Behrens *et al.* (*4*) showed that the Zn coverage dynamically responds to the chemical potential of the surrounding gas, which, for postreaction experiments, will be changed upon evacuation.

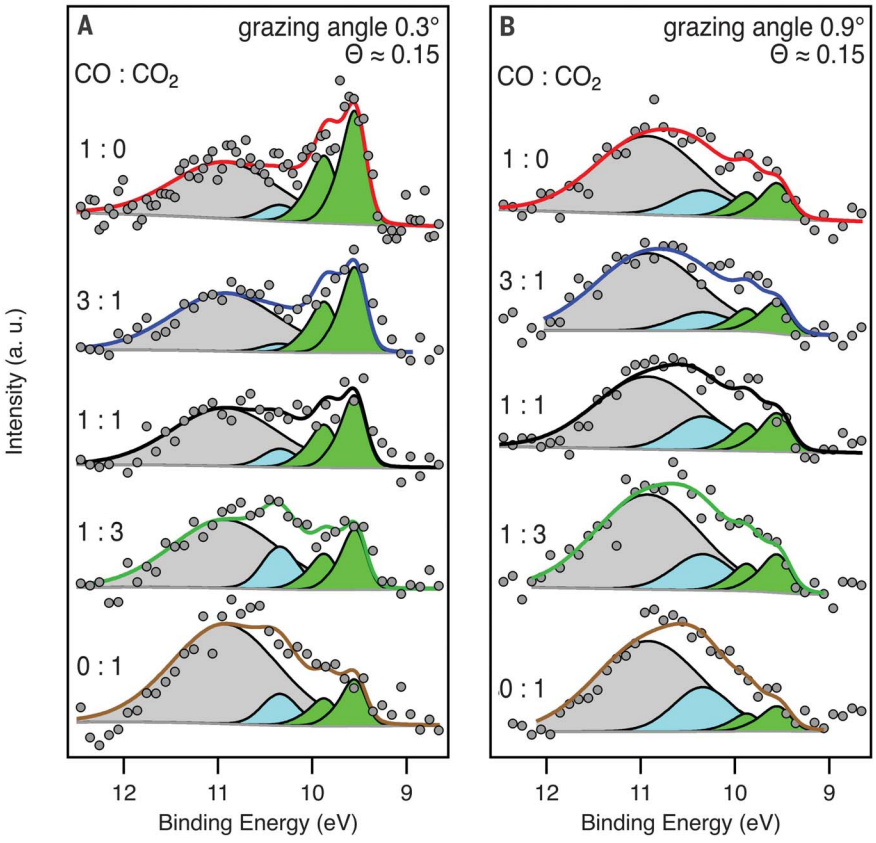

Fig. 2. Zn 3d spectral region in different gas compositions and probing depths. Spectra were collected at 180°C and ~280 mbar on the system Zn/ZnO/Cu(211) at a varying gas mixture of H_2:(CO + CO_2) = 2.6:1, with CO:CO_2 ratios indicated for ~15% surface Zn. Spectral raw data (circles) are deconvoluted by a four-peak structure. The green components at 9.53 and 9.85 eV correspond to the spin-orbit split components of metallic Zn 3d, the structure at 10.93 eV (gray) corresponds to ZnO, and the structure at 10.3 eV (light blue) corresponds to Zn in a (δ+) oxidation state. (**A**) Highly surface-sensitive experiments at a grazing incidence angle of 0.3°. A pronounced change is observed as the Zn:ZnO ratio varies. (**B**) Same experiment as in (A) but with a grazing incidence angle of 0.9°, to achieve greater bulk sensitivity. Data were accumulated consecutively, from CO:CO_2 = 1:0 to CO:CO_2 = 0:1. For each fixed-gas mixture, the angles of 0.3° and 0.9° were investigated.

In this work, we demonstrate that a specially engineered ambient-pressure XPS experiment, based on a design with local high pressure and extreme grazing incidence of incoming x-rays, is capable of providing high surface sensitivity (*25*). This approach enables investigation of the nature of Zn and surface-adsorbed intermediates with a pressure of several hundred millibar at elevated temperatures, thereby shifting toward more-realistic conditions for methanol synthesis. To enable a direct comparison with theoretical calculations (*4*) that aimed to describe the industrial catalytic process, we selected an identical model system with a stepped Cu(211) single crystal promoted by Zn. This system exhibits superior turnover frequency relative to other more-compact surfaces such as Cu(111) and Cu(100) (*4*, *6*).

Furthermore, the high concentration of steps at the surface acts to simulate defects, as motivated by the study of Behrens *et al.* (*4*). From Zn 3d core-level shifts, we found that the nature of Zn depended on the reaction gas mixture. Incidence angle–dependent spectra showed that, in CO_2-rich conditions, ZnO was favored to exist as bulk-like particles, whereas CO tended to generate metallic Zn that was alloyed with the Cu near the surface. From the C 1s spectra, we concluded that for CO_2 reduction there was a codominance of formate and methoxy as long-lived intermediates, whereas in CO the methoxy species dominated. The coverage of the intermediates diminished at higher temperature, indicating that the reaction was turning over. The aforementioned results support a model in which higher methanol production yield with a mixture of CO_2

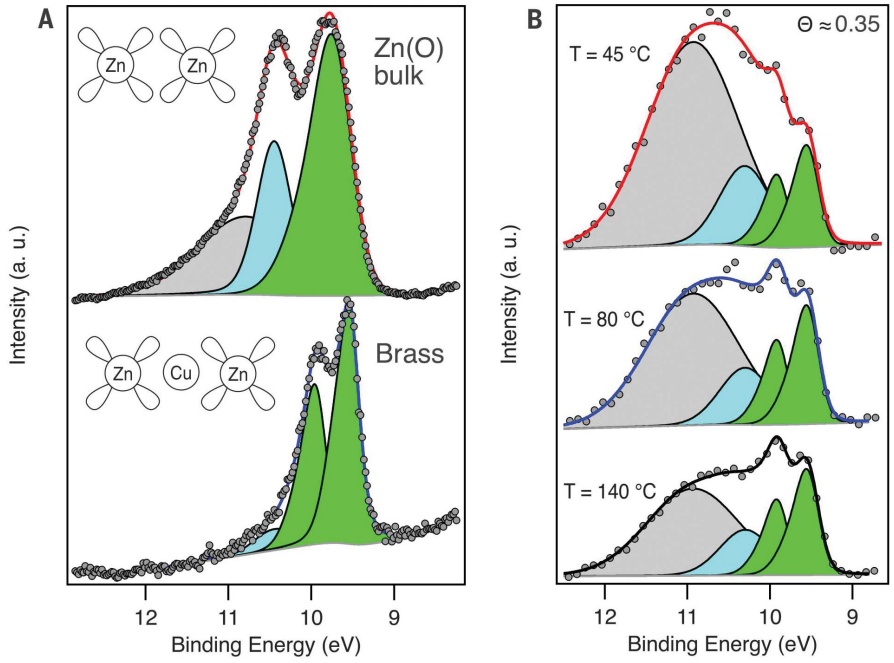

Fig. 3. Spin-orbit splitting in native polycrystalline ZnO_x and brass sample and temperature-dependent behavior of Zn on active Zn/ZnO/Cu(211). (**A**) Comparison of Zn 3d spectra measured in the hard x-ray photoelectron spectroscopy chamber at beamline P22, using a incidence angle of 5° to provide bulk-sensitive conditions. The spectra were recorded in vacuum conditions, with a photon energy of 4600 eV and at room temperature. Depending on the orbital overlap of neighboring Zn atoms, the $3d_{5/2}$-$3d_{3/2}$ spin-orbit splitting becomes apparent. (**B**) Temperature-dependent investigation of Zn/ZnO/Cu(211) with ~35% surface Zn under a grazing incidence angle of 0.6° and a stoichiometric gas ratio of H_2:CO = 2:1 at 180 mbar using the POLARIS instrument. Spectra accumulation took place in a consecutive manner from low to high temperature. Peak deconvolution and color coding are as in Fig. 2. The photon energy in this experiment was 4750 eV.

and CO (*3*) is a consequence of the strong reducing ability of CO, which generates a surface that has a high density of alloyed Cu-Zn sites (*3*) and is particularly active for CO_2 reduction to methanol (*2*).

Outline of the experiment

The principle of the experiment is illustrated in Fig. 1A (*26*). The Zn/ZnO/Cu(211) surface was prepared by evaporating metallic Zn and subsequent thermal annealing, generating around 15 or 35% of surface Zn inside the vacuum chamber without exposure to air [higher annealing temperature or longer annealing time led to less Zn surface content (*26*)]. The sample surface was then placed parallel to and within 30 μm of the electron spectrometer entrance. Precleaned and premixed gases of CO, CO_2, and H_2 were directed onto the sample surface, which created a localized volume of elevated pressure that acted as a small virtual cell with rapid gas flow. Using a well-focused and low-divergence x-ray beam from beamline P22 at the Petra III synchrotron radiation facility, we probed the surface under grazing incidence conditions with a precision of ±2 μrad (*25*). Given the specific reflectivity of the Cu single crystal, the choice of incidence angles below and above the critical angle of reflection allowed us to obtain depth information (*27*). To account for the variation in the pressure and differences in photoelectron absorption in the gas phase, all spectra were normalized to the simultaneously recorded Cu $2p_{3/2}$ core-level spectra. The measurements were conducted below a photon flux threshold so that beam-induced changes could be eliminated (*26*).

Owing to its high photoionization cross section, the stronger bound 2p core level is often used to determine the oxidation state of 3d metals. Previous studies focusing on the Zn $2p_{3/2}$ core level showed a shift from 1021.2 to 1021.8 eV upon oxidation of metallic Zn to ZnO (*6*), but the inherent lifetime broadening of the Zn $2p_{3/2}$ core level renders peak deconvolution highly ambiguous. However, the valence-like Zn 3d core level has less lifetime broadening and allows deconvolution into metallic and oxidized states (*28*, *29*), but with lower photoionization cross section and less signal intensity.

The importance of in situ measurements in comparison to postreaction analysis in vacuum has been demonstrated for CO_2-rich conditions (*26*). The spectra in fig. S4 show distinctly different peak positions, with a pronounced shift from oxidized Zn to more-metallic Zn under vacuum conditions (*7*). These findings emphasize the importance of in situ investigations, and we have conducted all of our experiments at pressures between 180 and 500 mbar.

Metallic Zn or ZnO depending on gas composition

In Fig. 1B we show Zn 3d spectra measured under reaction conditions of 180 mbar, 140°C, and 2:1 H_2:CO and 3:1 H_2:CO_2 gas fractions. The spectra were consistently characterized by four peaks at 10.9, 10.3, 9.8, and 9.5 eV throughout the accumulated dataset. As detailed below, the low–binding energy peaks at 9.5 and 9.8 eV (green) corresponded to the spin-orbit split states of metallic Zn $3d_{3/2}$ and Zn $3d_{5/2}$. We associated the broad structure at 10.9 eV (gray) with Zn in the +2 oxidation state, related to bulk-like ZnO. We assigned the component at ~10.3 eV (light blue) to a Zn-(δ+) oxidation state species related to Zn interacting with formate and methoxy (*4*, *30*, *31*) as well as some ZnOH. Thus, we identified the preferential states of Zn directly from the spectra under gas phase composition-dependent reaction conditions.

Under CO-rich conditions (H_2:CO = 2:1), the metallic Zn signal became more dominant (Zn:ZnO = 0.6), whereas under CO_2-rich conditions (H_2:CO_2 = 3:1), ZnO was strongly enhanced (Zn:ZnO = 0.34). When the pressure was increased to more-extreme conditions at 500 mbar and 230°C, the spectra became noisier, owing to increased gas-phase electron scattering (Fig. 1C), indicating that in pure CO metallic Zn was present almost exclusively, and in CO_2 only ZnO was observed. This observation directly indicated that CO promoted a more-reduced state enriched in metallic sites, whereas CO_2 drove the surface toward the fully oxidized state of Zn. We did not observe any evidence for the oxidation of Cu in either of these measurements (*26*).

The relative amount of Zn in at least two different redox states changes continuously in gas mixtures ranging from pure CO + H_2 mixture to pure CO_2 + H_2 mixture at 180°C and 280 mbar (Fig. 2). To distinguish the surface effects from bulk effects, we conducted separate measurements at two different incidence angles. At a grazing incidence angle of 0.3°, the effective probing depth was ~14 Å (*26*), which corresponded to between seven and eight layers, in accordance with the definition of interlayer distance from Gajdoš *et al.* (*32*). For 0.9° the probing depth was much greater (~53 Å) and corresponded to ~30 Cu layers. The response in peak intensity for the various gas mixtures (Fig. 2, A and B) resembles the situation discussed in connection with Fig. 1B: The peak structure under CO-rich

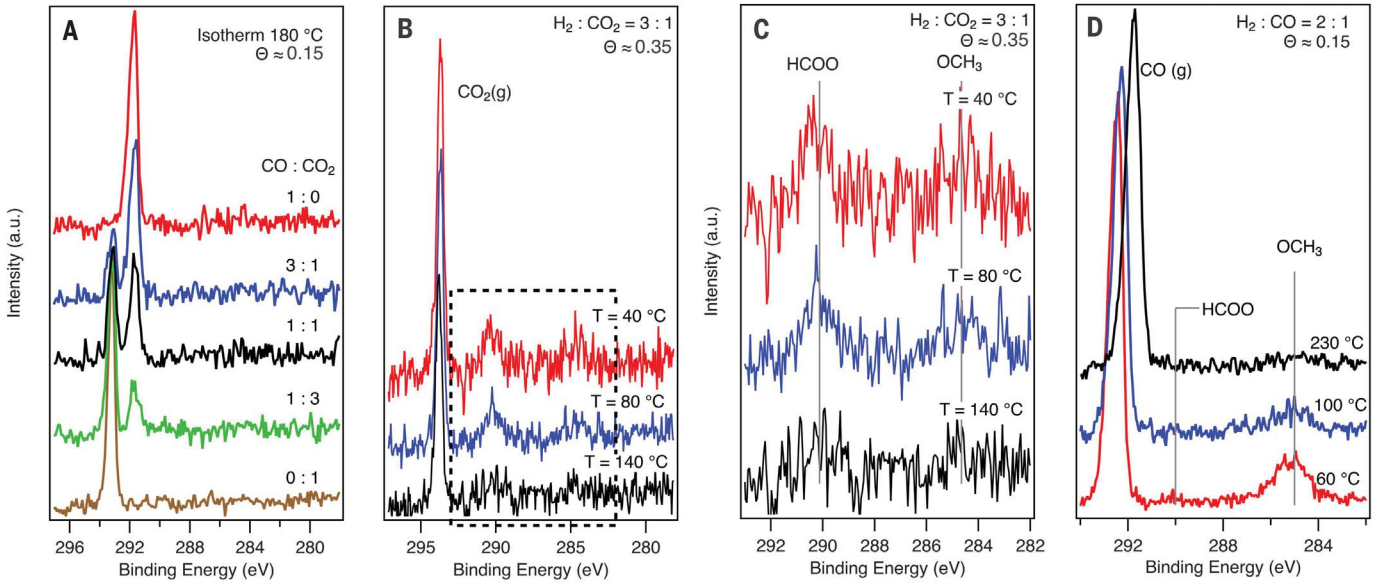

Fig. 4. Reaction intermediates probed in the C 1s region. (**A**) Surface-sensitive experiments at 180°C, ~230 mbar, and grazing incidence of 0.3°, with a varying gas mixture of H_2:(CO + CO_2) = 2.6:1. The spectra are characterized by two pronounced peaks in the region from 291 to 295 eV, corresponding to CO and CO_2 gas phase signals, and an otherwise featureless area between 278 and 291 eV. (**B**) X-ray photoelectron spectra at ~180 mbar and H_2:CO_2 = 3:1 at a grazing incidence angle of 0.6°. (**C**) Close-up view of the area surrounded by the dashed rectangle in (B), showing the presence of HCOO and OCH_3 reaction intermediates. (**D**) Spectra collected under temperature reduction in a mixture of H_2:CO = 2:1 and a pressure above ~470 mbar. For (A) and (D), data were collected with ~15% surface Zn; for (B) and (D), data were collected with ~35% surface Zn.

conditions is dominated by the metallic Zn component, whereas under CO_2-rich conditions the ZnO becomes dominant—but in all cases, we find a mixed state between metallic Zn and bulk-like ZnO_x. Because higher pressure induced more electron scattering, the spectra had a lower signal-to-noise level, the spin-orbit split peaks of the Zn 3d core level became less obvious, and the intensity of the fitted light blue Zn-(δ+) component became uncertain. The situation is distinctly different at a grazing incidence angle of 0.9° (Fig. 2B). The change in envelope peak structure was barely visible as the gas composition changed, and the relative signal from metallic Zn was weaker. Because we observed a higher metallic Zn signal in comparison to ZnO_x at more grazing incidence, we concluded that the reduction of ZnO to metallic Zn occurred in close proximity to the surface or directly at the surface, whereas the main fraction of ZnO_x should represent larger assemblies containing substantial bulk ZnO contributions. The Zn-ZnO_x reduction and oxidation were reproducibly independent of the direction upon switching between CO- and CO_2-rich conditions (fig. S5) (*26*).

Distinguishing Zn-Zn and Cu-Zn alloy interactions

We used the valence character of the Zn 3d electronic state to address the nature of Zn, distinguishing ZnO_x, metallic Zn islands on the surface, or a surface Cu-Zn alloy. Because the bandwidth of Zn 3d is determined by the overlapping atomic wave functions of neighboring atoms, the 3d bandwidth became larger with increased interaction between neighboring Zn atoms. By contrast, if the Zn atoms alloyed into Cu, with d states closer to the Fermi level, the Zn 3d would become more atomic in nature. If the 3d bandwidth was larger than the $3d_{5/2}$-$3d_{3/2}$ spin-orbit splitting, only one broad 3d peak would be seen, whereas if the width was smaller than the splitting, two 3d components would be seen (*33*). The Zn 3d spectra of native polycrystalline Zn and a $Zn_{37}Cu_{63}$ brass sample measured at an incidence angle of 5° (Fig. 3A) showed ZnO and intermediate ZnO_x redox states on top of the Zn bulk metal sample, but the steeper angle allowed probing of the underlying metallic Zn at 9.76 eV. For the native polycrystalline Zn in its metallic state, we indeed saw only a broad Zn 3d metal component resembling the aforementioned large-bandwidth case, with a broad 3d peak width. However, in the brass sample, two spin-orbit components centered at 9.95 and 9.56 eV were resolved, demonstrating that the alloying with Cu could lower the 3d bandwidth of Zn. These results provided a spectral fingerprint to distinguish ZnO_x, Zn interacting with Zn, and Zn interacting with Cu in the form of an alloy.

The Zn 3d spectra in Fig. 1B showed a spin-orbit split metallic feature that was enhanced under CO-rich conditions, which was indicative of a decrease in the Zn-Zn interaction. We interpreted the lower Zn-Zn interaction as alloying with Cu, similar to the brass sample. However, we could not rule out some Zn-Zn interaction, although the extent of coordination was small relative to the Zn-Cu interaction. This alloy formation was further promoted when the temperature was raised from 45° to 140°C (Fig. 3B). With increasing temperature, we noticed a strong change in the signal intensity related to the restructuring of the surface. The ZnO, which was initially on top of the Cu surface, broke up and transformed to Zn, which further alloyed into the Cu and increased the amount of surface-alloyed Zn from 7.8% at 45°C to 9.5% at 140°C. As the total amount of Zn with respect to Cu atoms decreased with increasing temperature, it appeared that some Zn was lost into the gas phase because of the high vapor pressure of Zn metal.

By contrast, Zn atoms in the alloy were thermally more stable. Preferentially, the alloying process would start at undercoordinated Cu sites such as step edges (*4*). Metallic Zn exhibits enhanced wetting on Cu that creates an even distribution of Zn atoms on the surface to maximize Zn-Zn distance. By contrast, ZnO tends to wet less and to accumulate into ZnO clusters or nanoparticles (*34*). For CO_2 reduction on Cu(111), Kattel *et al.*, Fujitani *et al.*, and Nakamura *et al.* showed that there is an optimum reactivity at a Zn coverage of ~20%

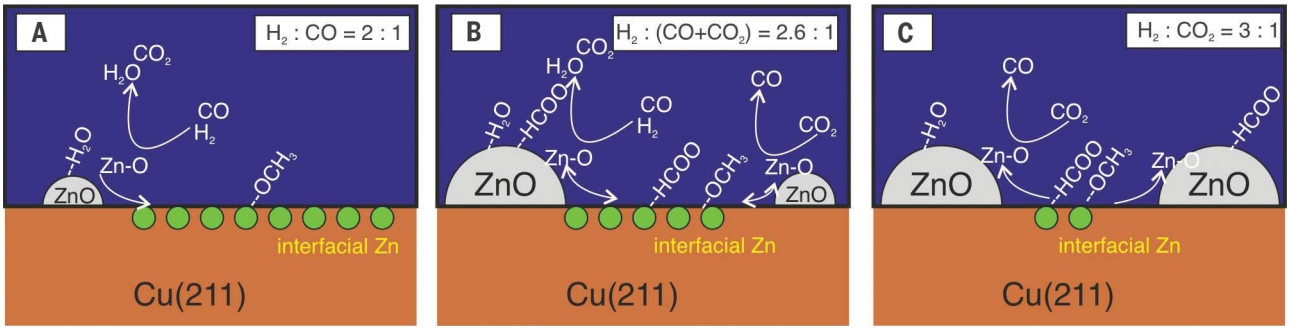

Fig. 5. Schematic illustration of the reaction mechanism. (**A** to **C**) Behavior of the Zn/ZnO/Cu(211) surface as dependent on reaction mixture and conditions, which range from CO-rich, reducing conditions in (A) to CO_2-rich, more-oxidizing conditions in (C). These illustrations show how temperature and gas mixture critically affect the ZnO ⇄ Zn equilibrium.

of monolayer and that the chemistry can be different above or below this value (*6*, *30*, *35*). Because the reaction plotted in Fig. 3B was conducted at Zn coverage above the optimum level, some Zn may not have formed surface alloys and was readily oxidized by water vapor. However, on a stepped Cu(211) surface with more active step sites (*4*), the optimum reactivity most likely occurred at a higher Zn coverage.

Stable reaction intermediates

We next consider the reaction mechanism and the identification of stable intermediates. Under steady-state conditions, it would be possible to detect only those long-lived intermediates that can give rise to a detectable population. Density functional theory predicts deep minima in the free-energy surface, with formation of formate and methoxy in the case of CO_2 hydrogenation and formation of only methoxy in the case of CO hydrogenation (*4*, *6*, *14*). We verified that CO_2 reduction proceeds through both formate and methoxy intermediates, whereas CO reduction proceeded predominantly through methoxy. Because the O 1s region of the intermediates exhibited overlapping ZnO and ZnOH peaks, we relied on the C 1s spectral region for identification, but the corresponding O 1s spectra are also shown for completeness (fig. S14) (*26*). Many different carbon-containing molecular species potentially populate the surface, and their binding energies depend on whether the coordination is with pure Cu sites, surface-alloyed Cu-Zn sites, pristine Zn sites, ZnO_x sites, or mixed Cu-ZnO_x sites. However, we note that a given binding energy position in the spectra is consistent with the proposed intermediates.

The C 1s spectra at 180°C and 230 mbar of H_2 with CO, CO_2, or mixtures of both reactants at a 0.3° incidence angle (Fig. 4A) showed strong peaks at ~293.2 and ~291.6 eV from gas-phase CO_2 and CO, respectively. The adsorbate region between 283 and 290 eV showed no peaks, meaning that the surface coverage of any carbon-containing species was very low, consistent with a high turnover rate and a lack of long-lived intermediates. At lower temperatures (≤140°C), the turnover rate decreased and intermediates became visible. For the reaction of CO_2 with H_2, adsorbates accumulated on the surface (Fig. 4, B and C). The coverage increased with decreasing temperature, and two broad spectral structures were observed at ~290 and ~285 eV. These adsorbate peaks could be consistently assigned to formate and methoxy species (*26*). We related the C 1s formate species to some of the intensity of the Zn-(δ+) peak at 10.3 eV in Figs. 1 and 2.

For CO hydrogenation, we saw a similar trend (Fig. 4D), with a peak at ~285.2 eV that increased with decreasing temperature. Such reactivity is consistent with methoxy as the predominant intermediate (*26*). There is not a straightforward interpretation for the peaks in the carbon region, but given that multiple species can coexist at various sites, we can rule out graphitic carbon as an intermediate, as it gives rise to a much narrower peak at a lower binding energy of 285.4 eV (*36*). We stress that the interpretation of formate and methoxy on ZnO and CuZn from CO_2 and methoxy on CuZn from CO is basically consistent with the proposed mechanisms of methanol synthesis (*4*, *6*, *14*) and has been observed in low-pressure or vacuum experiments (*7*, *24*, *30*, *37*–*40*).

Inferred surface-alloyed CuZn active sites for CO_2 reduction

A schematic representation of the "working" model catalyst is illustrated in Fig. 5. In situ XPS at pressures of ≥180 mbar provided insight into the dynamic changes of the surface-near redox chemistry during reaction conditions. By focusing on the Zn 3d level, we could disentangle the effects of gas-phase composition and temperature on the surface-alloyed Zn, (partially) oxidized states of Zn, and the stability of the system Zn/ZnO/Cu(211). This complexity explained the divergent descriptions of the system that arose from the use of different reaction mixtures (*2*, *41*) and the relative lack of in situ studies. Using different incidence angles, we conclude that, in the near-surface region, Zn can convert to a surface alloyed state, whereas ZnO remains within the bulk in the form of clusters or nanoparticles on the surface. Spectroscopically, we have demonstrated that Zn alloyed into the surface of Cu(211) to form a structure in which the Zn-Zn interaction is minimized. This observation is entirely consistent with the work of Behrens *et al.* (*4*), which suggests that Zn alloying into the Cu steps is energetically favorable.

With increasing temperature under reaction conditions, the surface gradually depleted formate and methoxy species, which is expected for a transient population of reaction intermediates. We inferred that the catalyst was very active in this state and that the observed low coverages were consistent with the findings of Kuld *et al.* (*3*). We conclude that the oxidation state of Zn was dictated by the redox chemical potential of the gas phase, rationalizing the autocatalytic behavior observed by Thrane *et al.* (*42*). Surface-alloyed Zn and ZnO_x acted as a dynamically reversible acceptor and donor, respectively, of O for the O atoms produced by the reductive activation of CO_2.

In a similar manner, Zn appeared to inhibit Cu oxidation, an effect related to the higher oxophilicity of Zn relative to Cu. Under CO-rich conditions (Fig. 5A), ZnO transformed into Zn at temperatures as low as 60°C by the formation of CO_2 and H_2O. If, alternatively, CO_2 is increasingly admixed to the reaction together with CO (Fig. 5B), it can access the active interfacial and/or metallic Zn sites and contribute to their oxidative depletion. The admixture of CO_2 to the reaction affected the local ZnO⇄Zn redox equilibrium by pushing it toward ZnO with increasing admixture of CO_2. In the absence of CO (Fig. 5C), mostly ZnO was stabilized and even enriched at 180°C.

Formation of ZnO occurred at the expense of an active alloyed surface, which was effectively needed for both product-forming reactions—CO_2 reduction and direct CO hydrogenation—to proceed.

We can conclude that the most-active state is stabilized in the simultaneous presence of balanced amounts of CO, CO_2, and H_2. An enhanced CO:CO_2 ratio kept the surface more metallic, and allowed methanol formation through CO_2 to proceed more efficiently, as seen from isotope labeling experiments (*16*). The results thereby indicate that the most-active state involved an optimized surface-near abundance of redox-active surface Zn-Cu alloy sites for the reduction of CO_2, fully consistent with the proposal from Behrens *et al.* (*4*) and other studies (*3*, *11*, *43*), whereas computation studies indicate that Zn poisons CO hydrogenation (*15*).

REFERENCES AND NOTES

1. G. A. Olah, *Angew. Chem. Int. Ed.* **44**, 2636–2639 (2005).
2. J. Sehested, *J. Catal.* **371**, 368–375 (2019).
3. S. Kuld *et al*., *Science* **352**, 969–974 (2016).
4. M. Behrens *et al*., *Science* **336**, 893–897 (2012).
5. M. S. Spencer, *Surf. Sci.* **192**, 329–335 (1987).
6. S. Kattel, P. J. Ramírez, J. G. Chen, J. A. Rodriguez, P. Liu, *Science* **355**, 1296–1299 (2017).
7. R. M. Palomino *et al*., *J. Phys. Chem. B* **122**, 794–800 (2018).
8. M. Zabilskiy *et al*., *Nat. Commun.* **11**, 2409 (2020).
9. A. Beck *et al*., *Nat. Catal.* **4**, 488–497 (2021).
10. N. J. Divins *et al*., *Nat. Commun.* **12**, 1435 (2021).
11. A. Le Valant *et al*., *J. Catal.* **324**, 41–49 (2015).
12. J. Nakamura *et al*., *Science* **357**, eaan8074 (2017).
13. S. Kattel, P. J. Ramírez, J. G. Chen, J. A. Rodriguez, P. Liu, *Science* **357**, eaan8210 (2017).
14. L. C. Grabow, M. Mavrikakis, *ACS Catal.* **1**, 365–384 (2011).
15. F. Studt *et al*., *ChemCatChem* **7**, 1105–1111 (2015).
16. G. C. Chinchen, P. J. Denny, J. R. Jennings, M. S. Spencer, K. C. Waugh, *Appl. Catal.* **36**, 1–65 (1988).
17. G. Ertl, H. Knözinger, J. Weitkamp, *Handbook of Heterogeneous Catalysis*, vols. 1 to 5 (Wiley, 2008).
18. R. Dalebout, N. L. Visser, C. E. L. Pompe, K. P. de Jong, P. E. de Jongh, *J. Catal.* **392**, 150–158 (2020).
19. A. Urakawa, *Nat. Catal.* **4**, 447–448 (2021).
20. I. Chorkendorff, J. W. Niemantsverdriet, *Concepts of Modern Catalysis and Kinetics* (Wiley, 2003).
21. M. Salmeron, R. Schlögl, *Surf. Sci. Rep.* **63**, 169–199 (2008).
22. D. E. Starr, Z. Liu, M. Hävecker, A. Knop-Gericke, H. Bluhm, *Chem. Soc. Rev.* **42**, 5833–5857 (2013).
23. J. Schnadt, J. Knudsen, N. Johansson, *J. Phys. Condens. Matter* **32**, 413003 (2020).
24. T. Koitaya *et al*., *ACS Catal.* **9**, 4539–4550 (2019).
25. P. Amann *et al*., *Rev. Sci. Instrum.* **90**, 103102 (2019).
26. Details of the materials and methods are available as supplementary materials.
27. L. G. Parratt, *Phys. Rev.* **95**, 359–369 (1954).
28. T. L. Barr, M. Yin, S. Varma, *J. Vac. Sci. Technol. A* **10**, 2383–2390 (1992).
29. K. Ozawa *et al*., *Surf. Sci.* **623**, 1–5 (2014).
30. T. Fujitani, I. Nakamura, T. Uchijima, J. Nakamura, *Surf. Sci.* **383**, 285–298 (1997).
31. Y. Shiozawa, T. Koitaya, K. Mukai, S. Yoshimoto, J. Yoshinobu, *J. Chem. Phys.* **152**, 044703 (2020).
32. M. Gajdoš, A. Eichler, J. Hafner, G. Meyer, K. H. Rieder, *Phys. Rev. B* **71**, 035402 (2005).
33. M. T. Greiner *et al*., *Nat. Chem.* **10**, 1008–1015 (2018).
34. D. Bikaljevic *et al*., *Appl. Catal. A Gen.* **572**, 151–157 (2019).
35. J. Nakamura, Y. Choi, T. Fujitani, *Top. Catal.* **22**, 277–285 (2003).
36. A. Nikitin, L. Å. Näslund, Z. Zhang, A. Nilsson, *Surf. Sci.* **602**, 2575–2580 (2008).
37. F. Raimondi, K. Geissler, J. Wambach, A. Wokaun, *Appl. Surf. Sci.* **189**, 59–71 (2002).
38. X. Deng *et al*., *Langmuir* **24**, 9474–9478 (2008).
39. A. V. Tarasov, F. Seitz, R. Schlögl, E. Frei, *ACS Catal.* **9**, 5537–5544 (2019).
40. I. Orozco *et al*., *J. Phys. Chem. C* **125**, 6673–6683 (2021).
41. M. Bowker, *ChemCatChem* **11**, 4238–4246 (2019).
42. J. Thrane *et al*., *Angew. Chem. Int. Ed.* **59**, 18189–18193 (2020).
43. D. Laudenschleger, H. Ruland, M. Muhler, *Nat. Commun.* **11**, 3898 (2020).

ACKNOWLEDGMENTS

We thank A. Gloskovskii for experimental support at the beamline and G. L. Silva Rodrigues and L. G. M. Pettersson for helpful discussions. **Funding:** This work was supported by the Swedish Research Council under grant no. 2013-8823, the Knut & Alice Wallenberg (KAW) foundation under grant no. 2016.0042, the Global Climate and Energy Project (GCEP) at Stanford University, and the Swedish Foundation for strategic research (Stiftelsen för Strategisk Forskning, SSF) under proj. nr. ITM 17-0034. We acknowledge DESY (Hamburg, Germany), a member of the Helmholtz Association HGF, for the provision of experimental facilities. Parts of this research were carried out at PETRA III using beamline P22. Beamtime was allocated for proposals I-2018014 EC and II-20190003 EC. **Author contributions:** P.A. and B.K. designed the study for beamtime I and II; P.A. and A.N. designed the study for beamtime III; P.A., B.K., and C.R. designed the experimental parameters for beamtime I, P.A. defined the parameters for beamtime II and III; P.A., B.K., C.R., N.K., and T.G. designed and implemented the evaporator; P.A., B.K., N.K., T.G., P.L., K.P., D.B., C.R., H.-Y.W., M.So., M.B., D.D., M.Sh., C.M.G., J.H.S., and J.G. conducted the experiments; P.A. analyzed the XPS data; D.D. analyzed the mass spectrometry data; P.A. created the figures; P.A., B.K., and A.N. interpreted the data; and P.A., A.N., B.K., and D.D. wrote the manuscript. **Competing interests:** The authors declare no competing interests. **Data materials availability:** All of the data necessary for evaluating the conclusions of the study are included in the supplementary materials.

SUPPLEMENTARY MATERIALS

science.org/doi/10.1126/science.abj7747
Materials and Methods
Supplementary Text
Figs. S1 to S16
Table S1
References (*44*–*55*)
Data S1

1 June 2021; resubmitted 9 December 2021
Accepted 29 March 2022
10.1126/science.abj7747

The state of zinc in methanol synthesis over a Zn/ZnO/Cu(211) model catalyst

Peter AmannBernhard KlötzerDavid DegermanNorbert KöpfleThomas GötschPatrick LömkerChristoph RameshanKevin PlonerDjuro BikaljevicHsin-Yi WangMarkus SoldemoMikhail ShipilinChristopher M. GoodwinJörgen GladhJoakim Halldin StenlidMia BörnerChristoph SchlueterAnders Nilsson

Science, 376 (6593), • DOI: 10.1126/science.abj7747

Zinc's state in methanol synthesis

Methanol can be synthesized from carbon monoxide (CO), carbon dioxide (CO), and molecular hydrogen (H) over copper–zinc (Cu–Zn) catalysts, but studies have disagreed about the chemical state of Zn. Although x-ray photoelectron spectroscopy (XPS) can determine its oxidation state, many studies have been limited to reaction pressures of a few millibars, where the rates are low. Amann *et al*. performed XPS at 180 to 500 millibars for CO and CO hydrogenation over a Zn/ZnO/Cu(211) surface at high turnover rates. Stoichiometric mixtures of CO and H formed ZnO, but for CO and H, Zn became more metallic and formed Cu alloys. In industrial synthesis, CO and H are mixed with CO, and the presence of CO would generate Cu–Zn alloy sites active for CO reduction to methanol. —PDS